

Short communication

A method for quantifying near range point source induced O₃ titration events using Co-located Lidar and Pandora measurements



Guillaume Gronoff^{a,b,*}, Joseph Robinson^{c,d}, Timothy Berkoff^a, Robert Swap^c, Betsy Farris^e, Jeremy Schroeder^f, Hannah S. Halliday^{a,g}, Travis Knepp^{a,b}, Elena Spinei^h, William Carrion^{a,b}, Edward E. Adcock^a, Zachary Johns^{a,i}, Danette Allen^a, Margaret Pippin^a

^a NASA Langley Research Center, Hampton, Va, USA

^b Science Systems and Applications Inc., Hampton, Va, USA

^c NASA Goddard Space Flight Center, Greenbelt, Md, USA

^d Joint Center for Earth Systems Technology, University of Maryland, Baltimore County, Md, USA

^e Mechanical Engineering, Colorado State University, Fort Collins, CO, USA

^f Geography and Planning, The University of Toledo, Toledo, OH, USA

^g Universities Space Research Association, Huntsville, AL, USA

^h Virginia Polytechnic Institute and State University, Blacksburg, VA, USA

ⁱ National Institute of Aerospace, Hampton, Va, USA

ARTICLE INFO

Keywords:

Lidar
O₃
Pandora
NO₂
Ship

ABSTRACT

A ground-based tropospheric O₃ lidar with unique vertical near-range capabilities was deployed in support of the larger OWLETS 2017 campaign on the Chesapeake Bay Bridge Tunnel, at the mouth of the Chesapeake Bay. It was sited in close proximity to a shipping channel with an ensemble of additional instrumentation including Pandora spectrometer systems, ozonesonde launches, and in-situ trace gas monitors – one flying on a drone. This unique combination enabled successful observation of a near-surface maritime ship plume emission event on August 01, 2017. The observations demonstrate an NO₂ enhancement coincident with O₃ depletion in the low altitude range of lidar data, allowing for quantification of ship plume height behavior as well as the evolution of trace-gas concentrations. The technological improvements enabling the observation are presented and discussed, demonstrating that a single observation platform would not have been able to fully capture and contextualize the emission event. This synergistic ground-based sampling approach shows great promise for future verification and validation of satellite air quality and atmospheric composition measurements.

1. Introduction

The world's estuaries are the confluence of human and natural activities with large human populations living in very close proximity to the goods and services provided by those estuaries. In the United States, approximately 40% of the population lives within 100 miles of the coast (<https://oceanservice.noaa.gov/facts/population.html>). The population living within the watershed of the largest and most productive estuary of the United States, the Chesapeake Bay (CB), is now greater than 18 million, an increase of more than 110% since 1960 (https://www.chesapeakebay.net/indicators/indicator/Chesapeake_bay_watershed_population). These populations and their associated anthropogenic activities impact not only the biogeochemistry of the watershed but also its associated air shed. Monitoring of air quality (AQ)

and atmospheric composition (AC) over and around complex coastal regions such as the CB represents a significant challenge for in-situ monitoring, satellite observations and associated modeling activities. Prior studies describe the need for observations not only in the horizontal but also vertical distributions in O₃ over the Chesapeake Bay to better understand its formation and redistribution within regional recirculation patterns (Martins et al., 2012; Goldberg et al., 2014; Loughner et al., 2011, 2014; Stauffer et al., 2015).

In an effort to characterize CB AQ variations, the Ozone Water Land Environmental Transition Study (OWLETS) campaign took place in July–August 2017 in the Tidewater region of Southeastern Virginia (Sullivan et al., 2019). The objective of the study was to obtain simultaneous measurements over water and land to characterize the AQ differences across the coastal boundary. To obtain over-water

* Corresponding author. NASA Langley Research Center, Hampton, Va, USA.

E-mail address: guillaume.p.gronoff@nasa.gov (G. Gronoff).

<https://doi.org/10.1016/j.atmosenv.2019.01.052>

Received 14 August 2018; Received in revised form 21 December 2018; Accepted 28 January 2019

Available online 19 February 2019

1352-2310/ © 2019 Elsevier Ltd. All rights reserved.

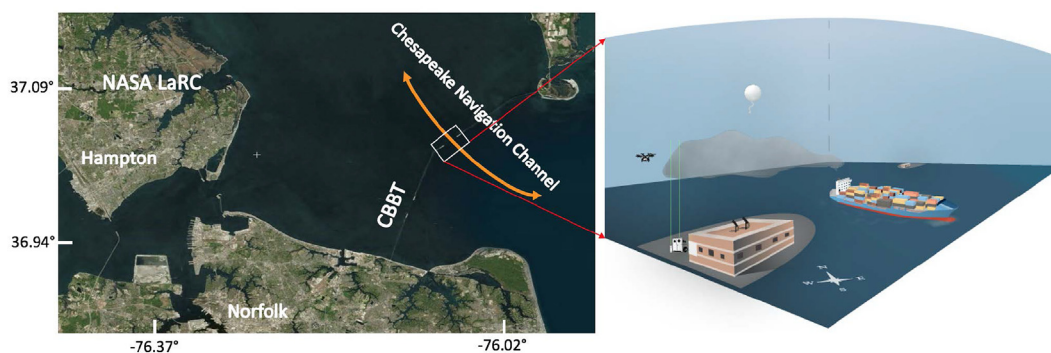


Fig. 1. Left) Enlarged satellite view of the OWLETS study area. The Chesapeake Bay Bridge Tunnel spans the mouth of the Bay and has the Chesapeake Navigation Channel with general ship paths marked in orange. Right) Schematic showing the Chesapeake Bay Bridge Tunnel measurement site and instrumentation during the passage of a large container vessel. (For interpretation of the references to color in this figure legend, the reader is referred to the Web version of this article.)

measurements, the NASA Langley Mobile Ozone Lidar (LMOL) (DeYoung et al., 2017) and a suite of supplemental measurements (e.g. Pandora Spectrometer Systems (Herman et al., 2009), Vaisala ceilometer (Eresmaa et al., 2006), Cimel sunphotometer (Holben et al., 1998) in addition to in-situ Ozone and NO₂ sensors) were deployed at a location along the Chesapeake Bay Bridge Tunnel (CBBT) ≈10 km offshore (Latitude 37.0365°, Longitude −76.0767° Fig. 1). The location was chosen as it was deemed to be an appropriate distance off-shore and downwind of the major urban center of greater Hampton, Va. Additionally, it was ideally situated, predominantly downwind on the south side of the Chesapeake Navigational Channel of the CBBT in close proximity to frequent maritime traffic. These observations were complimented by the NASA Goddard's Tropospheric Ozone Differential Absorption Lidar (TROPOZ) (Sullivan et al., 2014) along with ground-based measurements over-land at the NASA Langley Research Center (LaRC) in Hampton, Va. On observation days, time-synchronized data were collected that included launches of ozonesondes from both the CBBT and LaRC sites. Small Unmanned Aerial Systems (sUAS or UAV) outfitted with O₃ monitors were also deployed to complement the larger sampling suite by providing a greater sense of the spatial and temporal variability beyond fixed, ground-based samplers.

This combined deployment of synergistic platforms was a unique attempt to pilot ground-based AQ sampling packages in support of the verification and validation of satellites such as NASA's "Tropospheric Emissions: Monitoring Pollution" (TEMPO) mission (Zoogman et al., 2017) and/or ESA's Sentinel 5-Precursor with its Tropospheric Monitoring Instrument (TROPOMI) (Veefkind et al., 2012). This paper uses the case study of an observed plume emitted from a maritime freighter that passed from west to east through the Chesapeake Navigation Channel. This case study is used to assess the efficacy and synergistic power of instrument platforms deployed at the CBBT as part of OWLETS. Particular attention is paid to the advancements in the technology and engineering of the LMOL and the promise that this platform has to support ground-based, in-situ and satellite based AQ monitoring and research activities.

1.1. Ship plume impact on air quality

The quantity of freight moved by the international maritime has nearly quadrupled between 1970 and today to more than 10.3 billion metric tons annually (retrieved from <https://www.statista.com/statistics/234698/loaded-freight-in-international-maritime-trade-since-1970/>). This increase in freight has coincided with an increase not only in the number but also physical size of ocean-going freighters (such as the one in Fig. 2). These large ships are known to emit significant amounts of trace gas pollutants and O₃ precursors including nitrogen oxides (NO_x), sulfur oxides (SO_x), CO₂, CO, hydrocarbons, volatile organic compounds (VOC) and particulate matter (PM), all of which

impact AQ (Blasco et al., 2014; Moldanová et al., 2009). Agrawal et al. (2008); Corbett and Koehler (2003); Endresen et al. (2003) have estimated sea-going vessels account for ≈15% and ≈9% of all anthropogenic NO_x and SO_x emissions, respectively. Approximately 70% of these emissions occur within 400 km of the coast (Endresen et al., 2003; Eyring et al., 2005). This is a concern for regions surrounding ports and large shipping lanes due to associated environmental and health impacts (Corbett and Koehler, 2003; Eckhardt et al., 2013; Matthias et al., 2010; Najjar et al., 2010).

Large-scale transport models (Eckhardt et al., 2013; Huszar et al., 2010; Granier et al., 2006) are used to study the effects of ship emissions on the environment. However, these models are limited by the plume chemistry and dynamics assimilation. Cariolle et al. (2009) were able to better incorporate localized NO_x emissions into large scale atmospheric models by adjusting the non-linear behavior of NO_x reactions in plume chemistry. More recently, Ring et al. (2018) showed the impact of different plume input parameters on regional-scale O₃ densities using the Community Multiscale Air Quality Modeling System (CMAQ) (Byun and Schere, 2006). Ring et al. (2018) had to empirically modify the vertical emission profile (using vertical bins of ≈50 m) of large commercial marine vessel in the CMAQ model to better fit the observations of the HCHO/NO₂ ratio calculated from the Ozone Monitoring Instrument (OMI) data. High-resolution vertical observation of such plumes are therefore critical to better constrain model-satellite comparisons.

1.2. Ship plume chemistry

Maritime traffic has a complex impact on the local chemistry since their concentrated emissions can enhance or deplete some pollution markers on short time scales (Aliabadi et al., 2015; Eckhardt et al., 2013; Moldanová et al., 2009; Winnes and Fridell, 2010). One of these processes, the hindrance of O₃ production by emitted NO_x on short time scales and under various conditions, is understudied (Aliabadi et al., 2015). In the absence of precursor emissions, O₃ is in equilibrium with NO and NO₂ through the following reactions:



The volatile organic compounds (VOCs) can alter that equilibrium by producing NO₂ from NO without consuming an O₃.

The O₃ titration from combustion engines (Sillman, 1999) comes from the addition of large quantities of NO leading to dominance of the reaction: O₃ + NO → NO₂ + O₃. This standard atmospheric chemistry for emissions from combustion engines is sufficient for explaining the present observations. On the longer time scale, of the order of several



Fig. 2. Photograph of a large container vessel in the Chesapeake Bay during the OWLETS campaign. Note the brown exhaust plume. (For interpretation of the references to color in this figure legend, the reader is referred to the Web version of this article.)

hours, the NO_2 created is photo dissociated into NO while the extra oxygen reacts with O_3 to become O_3 again. The NO reacts with VOC and radicals (and not only O_3) to become NO_2 , which leads to the creation of more O_3 than what was present in the first place since typically, the NO_2 destruction pathways are slow (Brown and Stutz, 2012). The presence of the marine salt renders the problem more complex on the scale of several hours to days by increasing destruction rates of N_2O and Ox (Dickerson et al., 1999; Glasow et al., 2003; Brown and Stutz, 2012). Furthermore, it is important to take into account the temperature and the magnitude of the emission event: the emitted gases are at a higher temperature compared to the ambient surroundings, and therefore are buoyant, creating an aloft plume that can reach a few hundred meters in altitude. Several models of plume dispersion exist (Song et al., 2003; Chosson et al., 2008) but require validation through observation.

Previous campaigns dedicated to ship emission plume observations heavily relied upon aircraft measurements and Lagrangian measurement techniques (Chen et al., 2005; Sinha et al., 2003; Williams et al., 2009). While the measurement methods of those campaigns were able to provide precise concentrations of ship effluents, they focused on quantifying concentrations of pollutants and were not able to fully spatially contextualize the emission event. While the OWLETS campaign was not specifically designed to observe ship plumes, the sited instrumentation suite provided a unique fine-scale spatial and temporal resolution view of a ship plume event at the site. The work of Ring et al. (2018) shows that such observations with high spatial resolution are critical for improving models.

2. Instrumentation

The right panel of Fig. 1 is an artist view showing the instrumentation layout at the CBBT Third Island. A 2B Technologies 202 ground based ozone monitor were co-located at the LMOL trailer that was stationed next to the tunnel entrance building. Three Pandora Spectrometer Systems were mounted on the NW corner of the roof of the Third Island CBBT Building. Two had spectrometers to observe from 270 to 530 nm at .6 nm resolution and the third had a spectrometer to observe from 400 to 900 nm at 1.2 nm resolution. Balloon borne ozonesondes were launched from the end of the building closer to the channel and the UASs outfitted with 2B Technologies Personal Ozone Monitors (POM) were launched from the parking lot by the trailer. Details of key measurement platforms are given below.

2.1. The Langley Mobile Ozone Lidar (LMOL)

The Langley Mobile Ozone Lidar (LMOL) is a ground-based tropospheric profiling ozone lidar system, housed in a mobile trailer, has participated in air quality studies since 2014 (DeYoung et al., 2017).

LMOL is part of the NASA-sponsored Tropospheric Ozone Lidar Network (TOLNet <http://www-air.larc.nasa.gov/missions/TOLNet/>). TOLNet lidar systems have contributed to a wide range of atmospheric studies, including DISCOVER-AQ, FRAPPÉ CABOTS, FAST-LVOS, etc. (Wang et al., 2017; Sullivan et al., 2015; Johnson et al., 2018; Langford et al., 2018). As part of these efforts, TOLNet lidar teams have collectively developed rigorous instrument procedures and processing algorithms to ensure consistency in O_3 data products and associated uncertainties between instruments (Leblanc et al., 2016a, b). Cross-comparison studies conducted between TOLNet lidar systems (Leblanc et al., 2018; Wang et al., 2017; Sullivan et al., 2015) showed that O_3 profile concentrations typically agree within $\pm 5\%$, consistent with system specific propagated errors.

Like the other TOLNet lidar systems, LMOL relies on ultra-violet pulsed laser source that produces two wavelengths allowing for calculation of O_3 concentration profiles from atmospheric differential absorption (Browell et al., 1985). The LMOL laser transmitter consists of a custom-built Ce:LiCAF tunable UV oscillator (Fromzel et al., 2007) that is pumped by frequency doubled light from a commercial Q-switched 527 nm Nd:Yf laser. The transmitted pulsed output had a 1 kHz repetition rate, with pulses alternating between 287 and 292 nm that were propagated from the trailer roof in a zenith direction into the atmosphere. Backscattered light from the atmosphere was collected by two different co-aligned telescopes: the first being a 40 cm diameter Newtonian that was optimized for 1–8 km in altitude, and a second 7.5 cm diameter 90-deg off-axis parabolic mirror receiver that was optimized for signals in the 0.1–1 km range in altitude. Both receivers were fiber-coupled with a multi-mode fiber input aligned to the receiver field stop. The large and small receivers had a field-of-view of 1.5 and 15 mrad respectively, as defined by the telescope focal length and 1 mm fiber core-diameter used. The smaller diameter receiver was used for the first time during OWLETS to provide enhanced measurement capability in near-surface (0.1–1 km altitude) signal range. This set up has been validated against ozonedondes and sUAS in-situ data; a more detailed description of the systems and its performances is found in Farris et al. (2018). The fiber outputs from the near-field and far-field telescopes were coupled to collimating optics, UV bandpass filters (280–295 nm spectral window) that were integrated with Hamamatsu photo-multiplier tube (PMT) detectors in light-tight enclosures.

For normal atmospheric science data collection, the output of the PMTs were connected to a Licel data system that provided simultaneous analog and photon counting measurements of both the near-field and far-field PMT signals. The Licel system was synchronously gated with the alternating wavelength pulses, so that 286 and 292 nm wavelength profiles are separately captured by the data system memory and subsequently recorded to the computer data acquisition system for processing of raw signals into calibrated ozone profiles. The processing of

raw profile signals to obtain calibrated ozone profiles is implemented following the standard DIAL technique (Browell et al., 1985; DeYoung et al., 2017). Raws signals from both analog and photon counting are background subtracted and range-squared before applying a single-pass Savitzky-Golay filter (Leblanc et al., 2016b, and references therein); the more points used in the filter, the lower the resolution. Analog and photon-count channels are merged together to provide a single optimized profile for range and signal-to-noise performance (Leblanc et al., 2016b; Zhang et al., 2014; Newsom et al., 2009). Ozone cross sections along with pressure and temperature information are used as part of the filter process to extract ozone mixing ratio as a function of altitude. The process is repeated for each new profile on a 5 min temporal averaged basis, to provide a continuous curtain display on the evolution of ozone vertical distribution during the course of a day. From a data analysis perspective, the more the data are averaged vertically, the lower the noise, but at the expense of the vertical resolution. To facilitate comparisons with the TROPOZ lidar during OWLETS, a common vertical smoothing scheme has been used on both systems. For the current study, we performed an adaptive smoothing at 5%, i.e. the number of vertical smoothing points has been optimized for each altitude/profile to have the best vertical resolution possible while still being under 5% noise uncertainty, therefore not affecting the overall uncertainty in a significant way. This led to the acquisition of data in Fig. 3. The main drawback of the adaptive smoothing technique is the visible transition between lidar channels, in the current figure between the Very Near Field and the Far Field at 500 m.

2.2. Ground-based Pandora spectrometer system

Pandora is a ground-based UV–Visible spectrometer system capable of direct sun/moon and sky-scanning observations (Herman et al., 2009). Spectra collected by Pandora instruments are analyzed using Differential Optical Absorption Spectroscopy technique (DOAS) (Platt and Stutz, 2008). Depending on observation geometry, light detected by Pandora systems can travel different paths through the atmosphere allowing for detection of trace gas absorption at different altitudes. Direct sun/moon observation geometries result in total column absorption with minimal sensitivity to vertical profiles. Sky-scanning near horizon is mostly sensitive to absorption at the lower altitudes. Measurements in zenith direction provide information about stratospheric gas absorption at large solar zenith angles.

A full description of Pandora spectrometer system hardware and data processing is provided in Cede (2017). Briefly, each standard system consists of the following components: (1) a head sensor; (2) a two-axes positioner allowing for a 360°-azimuth and 90°-zenith range of

motion; (3) a fiber optic cable with 400 μm core diameter and numerical aperture of 0.22 to transmit photons to the spectrometer; (4) Avantes spectrometer (Model ULS2048x64, 280–520 nm) with a 50 μm slit, focal length of 75 mm and approximately a 0.6 nm resolution; (5) a temperature controller for the spectrometer enclosure and (6) a miniature Cincoze PC (Model DC-1100-R10) for instrument control, data logging and data transferring to the data server.

Pandora systems are calibrated spectrally and radiometrically in the laboratory. Characterized parameters include instrument dark current, nonlinearity, pixel response non-uniformity, dispersion, wavelength dependent slit function, stray light, filter transmission, and instrument temperature sensitivity. Post laboratory calibration, each Pandora is transferred to a testing platform at NASA/GSFC for 2-week observation in sun tracking mode. This is done to evaluate field performance of the instrument in comparison with reference Pandora systems. After instrument evaluation, the Pandora system is then shipped to the final deployment site. Weak absorbers (e.g. NO_2) require very high signal-to-noise ratio. To ensure this, a reference spectrum measured by Pandora at the deployment location is used. Determination of the gas abundance in the reference spectrum is based on the Modified Langley Extrapolation method and requires at least 2 weeks of relatively cloud free conditions at the deployment site. Until this “field” calibration is available a reference spectrum from GSFC is used to process the data. At the conclusion of its deployment, each instrument is tested again at GSFC for post-deployment evaluation. This allows for quality assurance based on instrument behavior before, during and after field deployment.

During normal operation as well as intensive field deployments, Pandora spectra are transferred to a server every 10 min as discussed in Cede (2017). They are then immediately processed and available for download. Data processing is done in four steps: 1) data correction for known instrumental artifacts; 2) calculation of slant column densities relative to the reference spectrum (DOAS fitting); 3) calculation of gas slant column density in the reference spectrum; and 4) conversion of slant column densities into total vertical column densities. Pandora NO_2 total column measurements have a precision of 0.002 DU with an accuracy of 0.1 DU and time resolution of 30–40 s. Previous work has shown this precision is sufficient enough to track short-term fluctuations in boundary layer NO_2 densities (Knepp et al. (2015)). Due to this sensitivity Pandora is suitable for monitoring of transient pollution sources, such as large shipping traffic and associated plumes.

For the purposes of the OWLETS campaign, the two NASA Pandora systems sited at CBBT were run in different sky scanning measurement modes. Pandora 40 was run in the standard sun/sky scanning mode with a total of 5 steps, leading to direct sun measurements approximately every 220 s. Pandora 19 was run in a mode that incorporated additional steps during its sky scanning, totaling 9 steps between direct sun measurements. This correlated to a direct sun measurement approximately once every 400 s.

2.3. The NASA Langley Research Center unmanned autonomous vehicles

OWLETS measurements included the use of a 2B Technologies POM sensor attached with a custom vibration isolated mount to the top of a battery operated octocopter sUAS that was operated by NASA LaRC's Autonomy Incubator team. The POM sensor used was a U.S. FEM approved and NIST traceable device (size: $0.1 \times 0.07 \times 0.04$ m, weight 0.45 kg) (2Btech, 2018b). The device calculates ozone concentration from optical absorption of UV light generated from a low pressure mercury lamp. The POM inlet consisted of a short length of Teflon tubing that included a manufacturer supplied filter. Pre-campaign characterization tests confirmed calibration accuracy better than $\pm 2\%$ when compared to a laboratory-based ozone generator and also showed similar accuracies during the campaign when compared to a surface sensor stationed at the CBBT site. Pre-mission flights were performed to verify that the sUAS did not compromise O_3 data and that the POM did

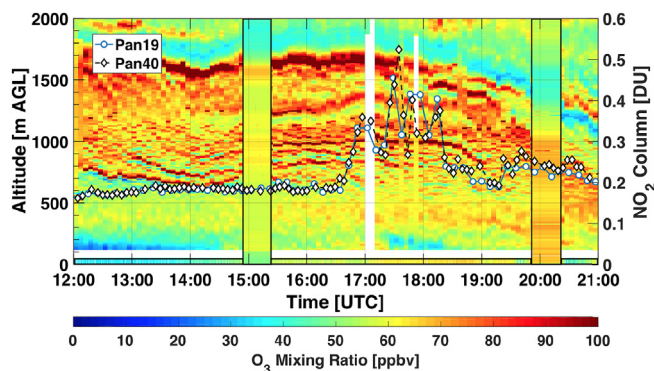


Fig. 3. Boundary layer O_3 lidar curtain obtained by LMOL between 12 and 24 UTC August 01, 2017. Vertical inserts represent two ozonesonde launches. Surface O_3 mixing ratios are shown by the horizontal insert at 0m. Pandora NO_2 column values from both instruments at CBBT are plotted on top of the curtain. Low altitude O_3 depletion and coincident NO_2 enhancement can be clearly seen at approximately 18 UTC.

not interfere with the flight electronics. Top mounting was important to avoid prop-wash from affecting the POM input, and also to maintain a clear GPS signal.

During sUAS flights approximately 15 min each, the POM sensor saved 10-s integrated O_3 concentrations along with GPS location and other instrument housekeeping information. Flights from the CBBT site were limited to 200 m in altitude and 1 km horizontal distance due to FAA airspace and NASA safety regulations. Adjacent to the CBBT was a shipping channel, and the allowed flight ranges were sufficient to directly sample the exhaust plumes from ships passing by the site. A secondary objective was to utilize the sUAS platform for vertical profiling up to 200 m over the lidar, to provide inter-comparisons with the lidar near-range data. As a result, flight patterns consisted of a combination of vertical and horizontal flights paths, that were selected depending on circumstances at the time. These flights were automated with waypoint loitering time corresponding to the sampling rate of the instrumentation.

2.4. Ground O_3 , NO_2 , and meteorological station

The OWLETS campaign used additional POM sensors as ground based instruments. These instruments were used as both stationary and traveling sensors, allowing the study of O_3 gradients along their path and the inter-calibration with the fixed instruments (Sullivan et al., 2019). Other ground based ozone monitors included the 2B Technology 202 instrument (2Btech, 2018a), which are based on the same technology as POM.

In addition to the ground ozone sensor, surface NO_2 was recorded using a Teledyne API model T500U Cavity Attenuated Phase Shift Spectrometer (CAPS). The T500U was granted Federal Equivalent Method status (Designation number EQNA-0514-212) in 2014. The T500U CAPS is a highly selective technique that provides a direct measurement of NO_2 , with a limit of detection of 40 ppt and precision of 0.5%. The CAPS method has been described in detail previously (Kebabian et al., 2005, 2007; 2008). Briefly, a 450 nm LED (± 10 nm) is square-wave modulated into a cavity of high-reflectivity mirrors, followed by detection on a vacuum photodiode. The detected signal is phase shifted proportional to the amount of NO_2 present in the cell, similar to the cavity ring-down technique. As opposed to standard chemiluminescence-based methods that are susceptible to NO_y , glyoxal, and HONO interference (Steinbacher et al., 2007; Sadanaga et al., 2010; Villena et al., 2012), CAPS is nearly interference free (Kebabian et al., 2008).

Several meteorological stations are located on the CBBT site for bridge safety monitoring and as routine measurement for NOAA. In this study, we used the data from the CHBV2 station of the NOAA buoy center (US Department of Commerce, 2018), located at 100 m from the lidar to the left of the CBBT island in Fig. 1, so that the CBBT building does not affect the wind speed and direction measurements in Fig. 4.

2.5. Ozonesondes

Coordinated O_3 (En-SCI, model 2Z-V7) and meteorological sonde (International Met Systems, iMet-1-ABXN) launches were performed at each sites (22 from LaRC, 20 from CBBT) [Knepp et al. in prep.]. This study utilized two sonde launches on August 01 at 15:00 and 21:00 UTC. Preflight conditioning for the O_3 sondes was performed in accordance with the Global Atmospheric Watch report (Smit and Panel, 2011) using the 0.5% buffer solution (Deshler et al., 2008). During flight, the standard NOAA pressure-dependent flow rate correction was applied (Johnson et al., 2002). The iMet radiosondes were outfitted with GPS, from which we were able to determine that the sondes were never further than 40 km from each other and never closer than 10 km. The atmospheric density and temperature profiles from these flights were used as input for the lidar retrieval, with the O_3 profile serving as validation of the retrieved product, following Leblanc et al. (2018).

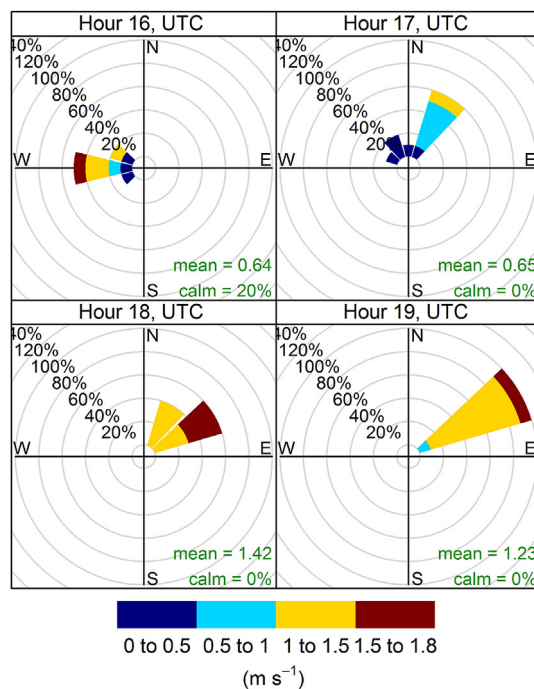


Fig. 4. Wind observation from the CBBT NOAA buoy.

Ozonesondes were compared against ground-based measurements, allowing to triple-check the calibration against yet another standard.

3. Emission plume and coincident ozone depletion event

As stated in Section 1, the CBBT site was adjacent to a shipping channel, and influenced by combustion emissions from cargo ships passing within 200–800 m of the site. Due to visual verification of a large cargo ship with a visible emission plume (Fig. 2), wind advection towards CBBT, and sUAS flight immediately after passage, this particular case presented itself for further analysis. Without optimizations in near surface observations by LMOL, this event would not and even could not, have been captured. Emissions from large ships like the one observed include NO , that can react with O_3 to produce NO_2 and temporarily reduce O_3 levels via the reactions described in Section 2. On August 1, 2017 between 16:30 and 18:30 UTC, an exhaust plume from a transiting maritime freighter was observed by the CBBT ensemble of measurement platforms.

Fig. 3 shows a snapshot of LMOL observations from 12:00 to 21:00 UTC on August 01 during a period when the LMOL system ran for more than 30 h continuously, retrieving atmospheric profiles of ozone with 5 min temporal resolution. During this period LMOL captured the complex evolution in vertical O_3 distribution, including boundary layer collapse (19–21 UTC), and fine structure residual layers from 0 to 1.5 km during the evening. During this time frame 2 ozonesonde were launched, and the O_3 profiles from these sondes are shown as the vertical inserts with surface O_3 data also plotted. Spatially co-located ozonesonde and sUAS O_3 results generally agree well (15%) with the lidar data (Farris et al., 2018), although there was only one set of ozonesonde data for comparison with LMOL data per 200 m height, due to the sensor time constant and ascent rate of the balloon.

The lowest altitude 0–300 m lidar data occasionally show depleted ozone events near the surface for relative short durations (up to an hour) that tend to correlate with column NO_2 data from the co-located Pandora instruments. In one of these cases, the sUAS in-situ sensor was flown horizontally over the channel just after passage of a large cargo ship (Fig. 2) on August 1 at 17:00 UTC.

Prior to the titration event NO_2 column amounts measured by both Pandora systems agreed extremely well with one another, to within a calculated average difference of 0.0004 DU. The local environment was homogeneous at this time, resulting in very steady NO_2 column observations. Further, this was despite the systems having different sampling routines that minimized temporally coincident direct sun observation opportunities. This difference in sampling schedule is visibly heightened with the observation of the dynamic exhaust plume as seen in Fig. 2. NO_2 column amounts increased sharply during the time from 16:30 to 19:00 UTC, with roughly a 0.2 DU enhancement observed during the passage of the plume at the height of O_3 titration. Additionally, the agreement between the two Pandora systems was still exceptional during this time, with a calculated average difference of 0.0028 DU between them. This strong agreement only serves to strengthen the LMOL/Pandora comparisons made when further investigating the August 01 event.

Fig. 4 shows the surface wind results obtained from the NOAA CHBV2 buoy, at 16:00, 17:00, 18:00, and 19:00 UTC illustrating winds originating from a northeasterly direction with varying speeds between 0 and 1.5 m/s with a mean at 0.65 m/s (US Department of Commerce, 2018). The sUAS flight took place from 16:53 to 17:16 UTC, taking off from the CBBT site, first ascending to 200 m in altitude and then horizontally transiting 1 km across the channel and then returning back towards CBBT at the same altitude. The in-situ O_3 data from the sUAS are shown in the outbound and return directions (grey overlays) in Fig. 5. It displays the time series of ozone and sUAS altitude during this flight. The first indication of the ship plume occurs at a distance 580 m from the CBBT site at 17:02 UTC, when the O_3 volume mixing ratio (vmr) quickly drops from 65 ppbv to 20 ppbv, and then returns back to 65 ppbv at 900 m distance. On the return path, O_3 vmr drops again, but in this case the first outbound transition edge is present 450 m from the island, indicating a movement of 130 m closer to the island in ≈ 228 s. This suggests an advection rate of 0.6 m/s rate towards the CBBT site, which is consistent with the wind direction and speed observations from the nearby buoy. At this rate, the plume is expected to arrive at the CBBT lidar at $\approx 17:20$ UTC.

An expanded view of O_3 lidar data from 17:20 to 19:30 UTC and 0–400 m in altitude are shown in Fig. 6a. As seen in the figure, a significant low altitude ozone depletion feature appears in this time frame, with a depletion maximum at 17:30 UTC. This O_3 depletion event correlates well in time with an increase in column NO_2 from both co-located Pandora instruments. The time series of both are shown in Fig. 6b. To compare the amount of O_3 concentration depletion with NO_2 generation associated with this feature, lidar O_3 data were integrated over 100–300 m in altitude to compute the total O_3 loss in time and converted to Dobson Units (DU, $\approx 2.687 \times 10^{20}$ molecules/m²). This corresponds to

$$\text{O}_3(t)_{\text{depleted}} = \text{Background} - \int_{100\text{ m}}^{300\text{ m}} \text{O}_3(t, z) \times \frac{N_a(t, z)}{\text{DU}} dz$$

where $\text{O}_3(t, z)$ is the value retrieved by the lidar at time t and altitude z in PPBV; N_a is the atmosphere number density in molecules per cubic meter; and the result is the amount of depleted O_3 in DU. The background values for non depleted O_3 and NO_2 were computed as the average between 19:00 and 19:30, as the data just prior to the plume was variable as resulting from natural causes along with the Pandora picking a part of the plume in advance due to its viewing angle. The lidar ozone depletion amount and NO_2 enhancement are displayed together on the same DU scale in Fig. 6c; the O_3 results are not sensitive to the background calculation, with the ozone differing by only a few percent different if taken before or after the plume, well under the uncertainty in the retrieval (of the order of 10%). The NO_2 background was typically 0.2 DU during the campaign, which is consistent with the value computed for this event. This clearly shows the event temporal correlation in trace gas concentrations. It also shows a good magnitude agreement in concentration changes since we have an increase of 0.2 DU in NO_2 that corresponds to the depletion of 0.2 DU of O_3 . During the depletion, the measured variability between the two Pandoras is approximately 0.05 DU. While there may be some uncertainty attributable to differences in the Pandora systems themselves, the dynamic and heterogeneous environment being sampled at slightly different times gives rise to subtle disparities in the Pandora total column measurements. Utilizing these assumptions, the calculated columnar O_3 depletion from LMOL agrees very well with the NO_2 enhancement measured by both Pandora systems.

The approximate balance in agreement between NO_2 production and O_3 depletion suggests the observed feature was driven entirely by the reaction $\text{NO} + \text{O}_3 \rightarrow \text{NO}_2$. From the aspect of the duration of the plume and its overall shape, the observed plume has an aloft duration of about an hour and an altitude of 100–200 m. The speed and nature of the ship, the nature of the winds and the boundary layer conditions affects these aspects (Chosson et al., 2008). The observed plume altitude and duration are within the bounds of the different simulations in Chosson et al. (2008) and, as a first approximation, our observed plume best matches the simulation for a convective steady state condition case (BOMEX case in Chosson et al. (2008)) with an initial mean buoyancy flux of 120 m⁴s⁻³.

In our particular case, the emission influence remained aloft just above the surface, as ground NO_2 and O_3 in-situ measurements did not observe this event as seen in Fig. 6d.

However, even in cases on non-surface influence, the presence of near surface pollutant concentrations are of interest to identify the impact of near-range variable point sources that may, if strong enough, be captured by satellite columnar observations and have comparison implications for models that typically rely on generalized fixed emission inventory data. In this regard the unique lidar-Pandora measurement

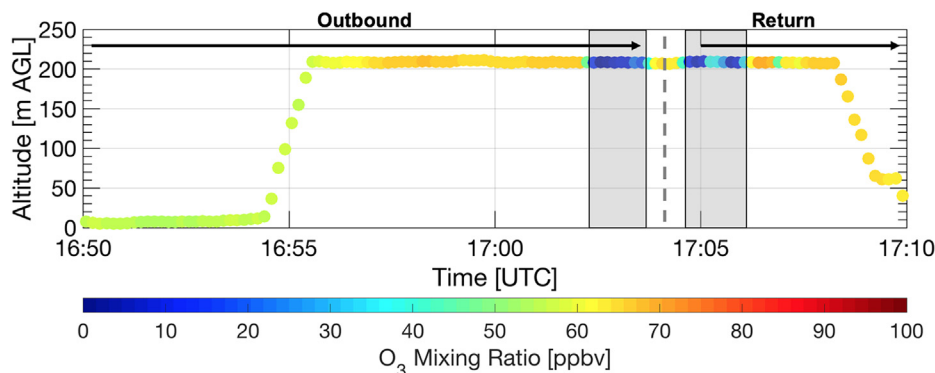


Fig. 5. Timeseries of sUAS flight over the channel on 2017 August 1. Data are colored by the observed O_3 mixing ratio from the onboard POM. The outbound and return periods of the flight are clearly marked, as are the two instances of observed depleted O_3 aloft (gray outlines).

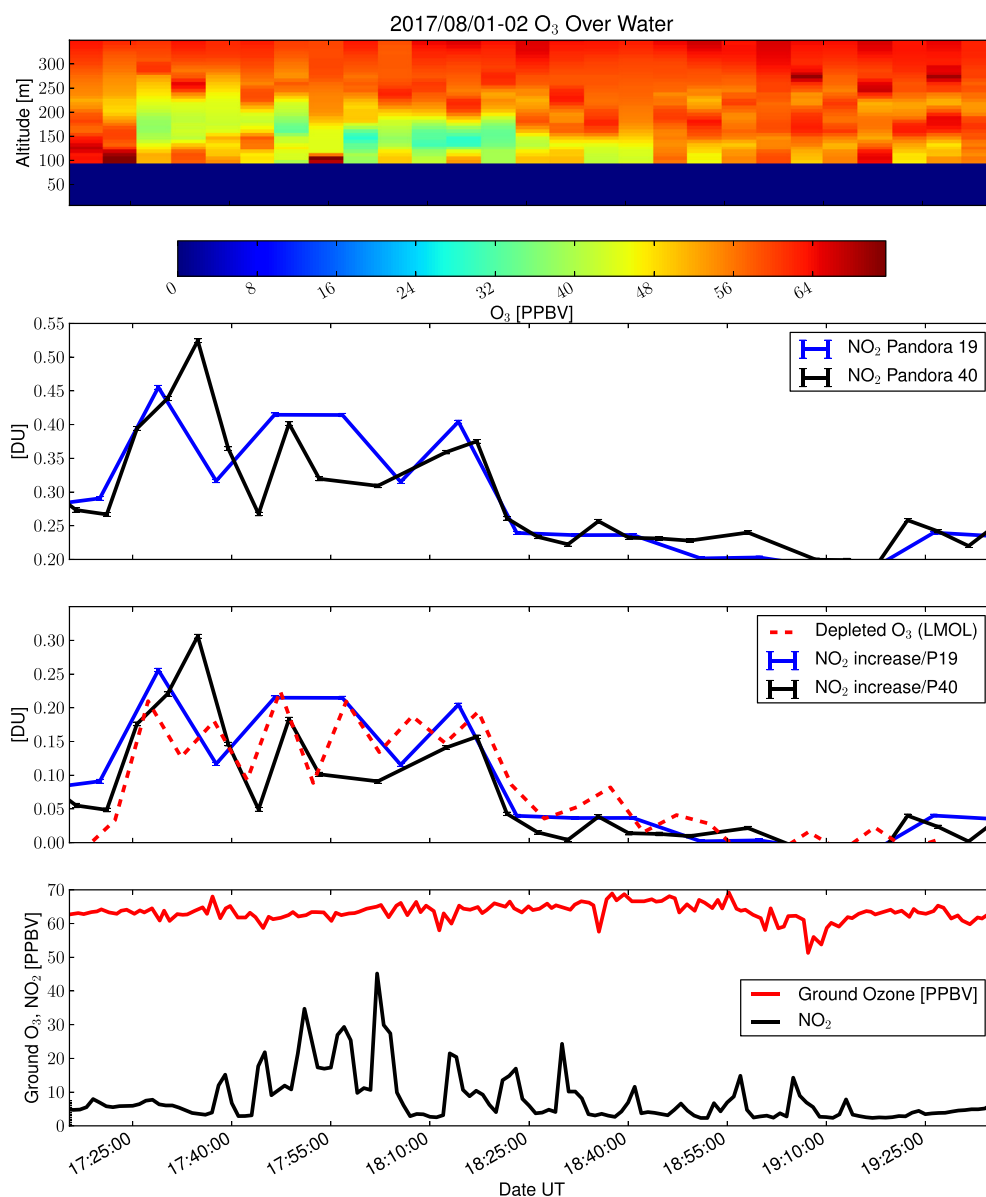


Fig. 6. Observation of the Titration Event by the Lidar and Pandora. Panel 1: LMOL vertical observations of O₃. Panel 2: Pandora observation of column NO₂. Panel 3: Amount of O₃ depleted along the increased amount of NO₂. Panel 4: Ground measurements of O₃ and NO₂.

approach provides a means to discern O₃ short duration titration events due to near-by point sources, identification of the corresponding NO₂ plume vertical distribution, and changes in concentration levels at the observation location.

4. Discussion/conclusion

The integrated lidar-Pandora co-located technique described here introduces a new approach for detection and characterization of near-range combustion plume events. Although characterization of cargo ship emissions was not the specific focus of the OWLETS campaign, the unique marine location adjacent to a shipping channel provided an opportunity to examine intermittent small scale emission events. This initial demonstration illustrates the potential of the combined retrieval approach, providing important insight into the source of O₃ variability occurring at the marine CBBT site occurring from shipping traffic versus other factors, such as the pollution transported from the nearby city of Norfolk, and the bay breeze recirculation (Sullivan et al., 2019). This can inform additional OWLETS analyses as well as future AQ/AC

campaigns. This will be an important consideration when comparing marine data to model predictions, since variability of short duration individual ship titration events are not normally represented in the National Air Quality Forecast Capability (NAQFC), or other CMAQ-based predictions. The August 1, 2017 case was evaluated because of the presence of favorable wind direction to bring a fresh plume to the observation site, with concurrent sUAS in-situ monitoring, and visual observation that allowed for a more detailed and unambiguous plume case to corroborate the lidar advancements and coupled Pandora analysis. As demonstrated by this case, quantitative NO₂ and O₃ concentration changes followed the expected behavior for high/saturated NO combustion plume conditions. This suggests concentration changes can be quantified for these events, in addition to identification and characterization of plume height dynamics. The combined NO₂ column, O₃ profile technique is most effective when there are stable signal levels before or after an event to provide adequate equilibrium state knowledge, sufficient NO generation for the NO₂ and O₃ influences to be seen within the noise limits of both instruments, and relatively uniform across any differing lidar-Pandora viewing geometries. The case study

presented here suggests cargo ship emissions can satisfy these conditions, but future work will be needed to investigate the full potential of this technique under a variety of conditions. This technique is likely to have applicability to other combustion point sources that generate fresh emissions, such as incinerators, power plants, forest fires, etc. As shown in Senff et al. (1998) large power plants plumes have already been observed using airborne lidar, or, as in Baidar et al. (2013), using a combination of an airborne instrument with a ground O₃ lidar. The technique presented here shows that much smaller plumes can be observed using mainly ground based instruments.

A coordinated observation of a pollution plume would optimally be done using co-located O₃ lidar, such as LMOL, and a NO₂ lidar such as the one described in (Volten et al., 2009). For logistical reasons (power availability, NO₂ lidar availability, authorization to transmit high powered visible laser in an environment with large flight traffic) it was not possible to perform an OWLET campaign with a NO₂ lidar. The technique presented here allowed to compensate for this lack of a dedicated NO₂ lidar using a more widely and easily available Pandora. The loss of vertical resolution in the Pandora was compensated here by the O₃ lidar data and the knowledge of chemistry.

In addition to Pandora, this approach may also be applicable when combining lidar O₃ data with other types of passive NO₂ column measurements, such as those from aircraft sensors including GeoTASO or ACAM either by overpassing a ground-based O₃ lidar or by co-locating with an aircraft O₃ lidar to achieve coincidental viewing geometry. The characterization of point source plume behavior is expected to not only assist in relating observational data to AQ models, but also benefit the evaluation satellite retrieval methods. Although multi-km satellite spatial footprint sizes such as those typical of TROPOMI and TEMPO are not expected to resolve point-source features, understanding variability, spatial dynamics, and vertical structure of point source plumes occurring within satellite spatial resolution limits is expected provide useful AQ insights. The potential of the combined remote sensing approach described here is integral for providing a more complete assessment of AC/AQ events (e.g. fresh emission plume events) and is expected to be further utilized in future studies to benefit field campaign analyses, leading to improvements in satellite retrievals and forecast models.

Declaration of interests

The authors declare that they have no known competing financial interests or personal relationships that could have appeared to influence the work reported in this paper.

Acknowledgements

The authors want to thank Dr. John Sullivan J. (NASA GSFC, Md, USA), Dr. Thierry Leblanc (JPL, Ca, USA), Alexander Kotsakis (USRA/NASA GSFC), Fernando Santos (CAPES), as well as two anonymous reviewers for useful discussions and comments. This work was supported by the 2017 NASA Science Innovation Fund. The authors gratefully acknowledge support provided by the NASA Tropospheric Composition Program, TEMPO Student Collaboration Project (supported by NASA Earth System Science Pathfinder Program), the NASA GSFC Pandora Project, the NASA AERONet Project, the Tropospheric Ozone Lidar Network (TOLNet). The OWLETS team would also like to thank the NOAA Environmental Modeling Center (EMC) and the NOAA Air Resources. Pandora deployment, operation and the near real time processing of data were collaboratively supported by the NASA ESD funded Pandora Project team (R. Swap, PI) out at GSFC in Greenbelt, MD, USA and by the ESA funded Pandonia team (A. Cede, PI) from Luftblick in Kreith, Austria. The Pandora Project would like to thank P. Pantina (SSAI/NASA GSFC) and A. Muhammand (NASA GSFC) for help in deployment of Pandora systems in support of OWLETS. The authors also acknowledge the support of the AERONET team from NASA GSFC

(Holben, PI). The authors would additionally like to thank Lindsey Flanary Hendrick, VCU Center for Environmental Studies, for her design of the CBBT measurement site schematic. This work could also not have been completed without the thoughtful accommodations of Edward Spencer and the entire Chesapeake Bay Bridge Tunnel Authority.

The data used for this study are publicly available on the OWLETS campaign website: <https://www-air.larc.nasa.gov/missions/owlets/index.html>.

Appendix A. Supplementary data

Supplementary data related to this article can be found at <https://doi.org/10.1016/j.atmosenv.2019.01.052>.

References

- 2Btech, 2018Ba. 2B 202. <https://twobtech.com/model-202-ozone-monitor.html>. <https://twobtech.com/model-202-ozone-monitor.html>.
- 2Btech, 2018Bb. POM, Personal Ozone Monitor. (<http://twobtech.com/pom-personal-ozone-monitor.html>). <http://twobtech.com/pom-personal-ozone-monitor.html>.
- Agrawal, H., Malloy, Q.G., Welch, W.A., Miller, J.W., Cocker, D.R., 2008. In-use gaseous and particulate matter emissions from a modern ocean going container vessel. *Atmos. Environ.* 42 (21), 5504–5510. <http://www.sciencedirect.com/science/article/pii/S1352231008002057>.
- Aliabadi, A.A., Staebler, R.M., Sharma, S., 2015. Air quality monitoring in communities of the canadian arctic during the high shipping season with a focus on local and marine pollution. *Atmos. Chem. Phys.* 15 (5), 2651–2673. <https://www.atmos-chem-phys.net/15/2651/2015/>.
- Baidar, S., Volkamer, R., Alvarez, R., Brewer, A., Davies, F., Langford, A., Oetjen, H., Pearson, G., Senff, C., Hardesty, R.M., 2013. Combining active and passive airborne remote sensing to quantify no₂ and ox production near bakersfield, ca. *Br. J. Environ. Clim. Change* 3 (4), 566.
- Blasco, J., Durán-Grados, V., Hampel, M., Moreno-Gutiérrez, J., 2014. Towards an integrated environmental risk assessment of emissions from ships' propulsion systems. *Environ. Int.* 66, 44–47. <http://www.sciencedirect.com/science/article/pii/S0160412014000191>.
- Browell, E.V., Ismail, S., Shipley, S.T., Sep 1985. Ultraviolet dial measurements of o₃ profiles in regions of spatially inhomogeneous aerosols. *Appl. Opt.* 24 (17), 2827–2836. <http://ao.osa.org/abstract.cfm?URI=ao-24-17-2827>.
- Brown, S.S., Stutz, J., 2012. Nighttime radical observations and chemistry. *Chem. Soc. Rev.* 41, 6405–6447. <https://doi.org/10.1039/C2CS35181A>.
- Byun, D., Schere, K.L., 2006. Review of the governing equations, computational algorithms, and other components of the models-3 community Multiscale Air quality (CMAQ) modeling system. *Appl. Mech. Rev.* 59, 51.
- Cariolle, D., Caro, D., Paoli, R., Hauglustaine, D.A., Cuénot, B., Cozic, A., Paugam, R., 2009. Parameterization of plume chemistry into large-scale atmospheric models: application to aircraft NOx emissions. *J. Geophys. Res.: Atmos.* 114 (D19) n/a–n/a, d19302. <https://doi.org/10.1029/2009JD011873>.
- Cede, A., Apr. 2017. Manual for Blick Software suite 1.3. Tech. Rep. 7. LUFTBLICK Earth Observation Technologies. http://pandonia.net/media/documents/BlickSoftwareSuite_Manual_7.pdf.
- Chen, G., Huey, L.G., Trainer, M., Nicks, D., Corbett, J., Ryerson, T., Parrish, D., Neuman, J.A., Nowak, J., Tanner, D., Holloway, J., Brock, C., Crawford, J., Olson, J.R., Sullivan, A., Weber, R., Schauffler, S., Donnelly, S., Atlas, E., Roberts, J., Flocke, F., Hbler, G., Fehsenfeld, F., 2005. An investigation of the chemistry of ship emission plumes during ITCT 2002. *J. Geophys. Res.: Atmos.* 110 (D10) n/a–n/a, d10S90. <https://doi.org/10.1029/2004JD005236>.
- Chosson, F., Paoli, R., Cuenot, B., 2008. Ship plume dispersion rates in convective boundary layers for chemistry models. *Atmos. Chem. Phys.* 8 (16), 4841–4853. <https://www.atmos-chem-phys.net/8/4841/2008/>.
- Corbett, J.J., Koehler, H.W., 2003. Updated emissions from ocean shipping. *J. Geophys. Res.: Atmos.* 108 (D20) n/a–n/a, 4650. <https://doi.org/10.1029/2003JD003751>.
- Deshler, T., Mercer, J.L., Smit, H.G.J., Stubi, R., Levrat, G., Johnson, B.J., Oltmans, S.J., Kivi, R., Thompson, A.M., Witte, J., Davies, J., Schmidlin, F.J., Brothers, G., Sasaki, T., FEB 29 2008. Atmospheric comparison of electrochemical cell ozonesondes from different manufacturers, and with different cathode solution strengths: the Balloon Experiment on Standards for Ozonesondes. *J. Geophys. Res.-Atmos.* 113 (D4).
- DeYoung, R., Carrion, W., Ganoe, R., Pliutau, D., Gronoff, G., Berkoff, T., Kuang, S., Jan 2017. Langley mobile ozone lidar: ozone and aerosol atmospheric profiling for air quality research. *Appl. Opt.* 56 (3), 721–730. <http://ao.osa.org/abstract.cfm?URI=ao-56-3-721>.
- Dickerson, R.R., Rhoads, K.P., Carsey, T.P., Oltmans, S.J., Burrows, J.P., Crutzen, P.J., 1999. Ozone in the remote marine boundary layer: a possible role for halogens. *J. Geophys. Res.: Atmos.* 104 (D17), 21385–21395. <https://doi.org/10.1029/1999JD900023>.
- Eckhardt, S., Hermansen, O., Grythe, H., Fiebig, M., Stebel, K., Cassiani, M., Baecklund, A., Stohl, A., 2013. The influence of cruise ship emissions on air pollution in Svalbard – a harbinger of a more polluted Arctic? *Atmos. Chem. Phys.* 13 (16), 8401–8409. <https://www.atmos-chem-phys.net/13/8401/2013/>.

- Endresen, O., Sorgard, E., Sundet, J.K., Dalsoren, S.B., Isaksen, I.S.A., Berglen, T.F., Gravir, G., 2003. Emission from international sea transportation and environmental impact. *J. Geophys. Res.: Atmos.* 108 (D17), 4560. <https://doi.org/10.1029/2002JD002898>.
- Eresmaa, N., Karppinen, A., Joffe, S.M., Räsänen, J., Talvitie, H., 2006. Mixing height determination by ceilometer. *Atmos. Chem. Phys.* 6 (6), 1485–1493. <https://www.atmos-chem-phys.net/6/1485/2006/>.
- Eyring, V., Köhler, H.W., van Aardenne, J., Lauer, A., 2005. Emissions from international shipping: 1. the last 50 years. *J. Geophys. Res.: Atmos.* 110 (D17) n/a–n/a, d17305. <https://doi.org/10.1029/2004JD005619>.
- Farris, B.M., Gronoff, G.P., Carrion, W., Knepp, T., Pippin, M., Berkoff, T.A., 2018. Demonstration of an off-axis parabolic receiver for near-range retrieval of lidar ozone profiles. In: *Atmospheric Measurement Techniques Discussions* –accepted in *Atmospheric Measurement Techniques* 2018, pp. 1–11. <https://www.atmos-meas-tech-discuss.net/amt-2018-178/>.
- Frommel, V.A., Prasad, C.R., Petrosyan, K.B., Liaw, Y., Wenhui, S., Yakshin, M., DeYoung, R., May 2007. Rapidly tunable, narrow linewidth, 1w, 1 khz ce:licaf laser pumped by the fourth harmonic of a diode-pumped nd:yf laser for ozone dial measurements. In: *2007 Conference on Lasers and Electro-Optics (CLEO)*, pp. 1–2.
- Glasow, R. v., Lawrence, M., Sander, R., Crutzen, P., 2003. Modeling the chemical effects of ship exhaust in the cloud-free marine boundary layer. *Atmos. Chem. Phys.* 3 (1), 233–250.
- Goldberg, D.L., Loughner, C.P., Tzortziou, M., Stehr, J.W., Pickering, K.E., Marufu, L.T., Dickerson, R.R., 2014. Higher surface ozone concentrations over the Chesapeake bay than over the adjacent land: observations and models from the discover-aq and cbodaq campaigns. *Atmos. Environ.* 84, 9–19. <http://www.sciencedirect.com/science/article/pii/S1352231013008364>.
- Granier, C., Niemeier, U., Jungclaus, J.H., Emmons, L., Hess, P., Lamarque, J.-F., Walters, S., Brasseur, G.P., 2006. Ozone pollution from future ship traffic in the arctic northern passages. *Geophys. Res. Lett.* 33 (13) n/a–n/a, l13807. <https://doi.org/10.1029/2006GL026180>.
- Herman, J., Cede, A., Spinei, E., Mount, G., Tzortziou, M., Abuhassan, N., 2009. NO₂ column amounts from ground-based Pandora and MFDOS spectrometers using the direct-sun DOAS technique: intercomparisons and application to OMI validation. *J. Geophys. Res.: Atmos.* 114 (D13), d13307. <https://doi.org/10.1029/2009JD011848>.
- Holben, B.N., Eck, T.F., Slutsker, I., Tanre, D., Buis, J., Setzer, A., Vermote, E., Reagan, J., Kaufman, Y., Nakajima, T., et al., 1998. AERONET—A federated instrument network and data archive for aerosol characterization. *Rem. Sens. Environ.* 66 (1), 1–16.
- Huszar, P., Cariolle, D., Paoli, R., Halenka, T., Belda, M., Schlager, H., Miksovsky, J., Pisoft, P., 2010. Modeling the regional impact of ship emissions on no_x and ozone levels over the eastern Atlantic and western Europe using ship plume parameterization. *Atmos. Chem. Phys.* 10 (14), 6645–6660. <https://www.atmos-chem-phys.net/10/6645/2010/>.
- Johnson, B., Oltmans, S., Vomel, H., Smit, H., Deshler, T., Kroger, C., SEP-OCT 2002. Electrochemical concentration cell (ECC) ozonesonde pump efficiency measurements and tests on the sensitivity to ozone of buffered and unbuffered ECC sensor cathode solutions. *J. Geophys. Res.: Atmos.* 107 (D19) ACH 8–1–ACH 8–18.
- Johnson, M.S., Liu, X., Zoogman, P., Sullivan, J., Newchurch, M.J., Kuang, S., Leblanc, T., McGee, T., 2018. Potential sources of a priori ozone profiles for tempo tropospheric ozone retrievals. *Atmos. Meas. Tech. Discuss.* 2018, 1–33. <https://www.atmos-meas-tech-discuss.net/amt-2017-484/>.
- Kebabian, P.L., Robinson, W.A., Freedman, A., JUN 2007. Optical extinction monitor using cw cavity enhanced detection. *Rev. Sci. Instrum.* 78 (6).
- Kebabian, P.L., Wood, E.C., Herndon, S.C., Freedman, A., AUG 15 2008. A practical alternative to chemiluminescence-based detection of nitrogen dioxide: cavity attenuated phase shift spectroscopy. *Environ. Sci. Technol.* 42 (16), 6040–6045.
- Kebabian, P., Herndon, S., Freedman, A., JAN 15 2005. Detection of nitrogen dioxide by cavity attenuated phase shift spectroscopy. *Anal. Chem.* 77 (2), 724–728.
- Knepp, T., Pippin, M., Crawford, J., Chen, G., Szykman, J., Long, R., Cowen, L., Cede, A., Abuhassan, N., Herman, J., Delgado, R., Compton, J., Berkoff, T., Fishman, J., Martins, D., Stauffer, R., Thompson, A.M., Weinheimer, A., Knapp, D., Montzka, D., Lenschow, D., Neil, D., Sep 2015. Estimating surface no₂ and so₂ mixing ratios from fast-response total column observations and potential application to geostationary missions. *J. Atmos. Chem.* 72 (3), 261–286. <https://doi.org/10.1007/s10874-013-9257-6>.
- Langford, A.O., Alvarez, R.J., Brioude, J., Evan, S., Iraci, L.T., Kirgis, G., Kuang, S., Leblanc, T., Newchurch, M.J., Pierce, R.B., Senff, C.J., Yates, E.L., Feb. 2018. Coordinated profiling of stratospheric intrusions and transported pollution by the tropospheric ozone lidar network (TOLNet) and NASA alpha jet experiment (AJAX): observations and comparison to HYSPLIT, RAQMS, and FLEXPART. *Atmos. Environ.* 174, 1–14.
- Leblanc, T., Sica, R.J., van Gijssel, J.A.E., Godin-Beekmann, S., Haefele, A., Trickl, T., Payen, G., Gabarrot, F., 2016a. Proposed standardized definitions for vertical resolution and uncertainty in the ndacc lidar ozone and temperature algorithms – part 1: vertical resolution. *Atmos. Meas. Tech.* 9 (8), 4029–4049. <https://www.atmos-meas-tech.net/9/4029/2016/>.
- Leblanc, T., Sica, R.J., van Gijssel, J.A.E., Godin-Beekmann, S., Haefele, A., Trickl, T., Payen, G., Liberti, G., 2016b. Proposed standardized definitions for vertical resolution and uncertainty in the ndacc lidar ozone and temperature algorithms – part 2: ozone dial uncertainty budget. *Atmos. Meas. Tech.* 9 (8), 4051–4078. <https://www.atmos-meas-tech.net/9/4051/2016/>.
- Leblanc, T., Brewer, M.A., Wang, P.S., Granados-Muñoz, M.J., Strawbridge, K.B., Travis, M., Firanski, B., Sullivan, J.T., McGee, T.J., Sunnicht, G.K., Twigg, L.W., Berkoff, T.A., Carrion, W., Gronoff, G., Aknan, A., Chen, G., Alvarez, R.J., Langford, A.O., Senff, C.J., Kirgis, G., Johnson, M.S., Kuang, S., Newchurch, M.J., Nov. 2018. Validation of the TOLNet lidars: the southern California ozone observation Project (SCOOP). *Atmos. Meas. Tech.* 11, 6137–6162.
- Loughner, C.P., Allen, D.J., Pickering, K.E., Zhang, D.-L., Shou, Y.-X., Dickerson, R.R., 2011. Impact of fair-weather cumulus clouds and the Chesapeake bay breeze on pollutant transport and transformation. *Atmos. Environ.* 45 (24), 4060–4072. <http://www.sciencedirect.com/science/article/pii/S1352231011003591>.
- Loughner, C.P., Tzortziou, M., Follette-Cook, M., Pickering, K.E., Goldberg, D., Satam, C., Weinheimer, A., Crawford, J.H., Knapp, D.J., Montzka, D.D., Diskin, G.S., Dickerson, R.R., 2014. Impact of bay-breeze circulations on surface air quality and boundary layer export. *J. Appl. Meteorol. Climatol.* 53 (7), 1697–1713. <https://doi.org/10.1175/JAMC-D-13-0323.1>.
- Martins, D.K., Stauffer, R.M., Thompson, A.M., Knepp, T.N., Pippin, M., 2012. Surface ozone at a coastal suburban site in 2009 and 2010: relationships to chemical and meteorological processes. *J. Geophys. Res.: Atmos.* 117 (D5), d05306. <https://doi.org/10.1029/2011JD016828>.
- Matthias, V., Bewersdorff, I., Aulinger, A., Quante, M., 2010. The contribution of ship emissions to air pollution in the north sea regions. *Environ. Poll.* 158 (6), 2241–2250. Advances of air pollution science: from forest decline to multiple-stress effects on forest ecosystem services. <http://www.sciencedirect.com/science/article/pii/S0269749110000746>.
- Moldanová, J., Fridell, E., Popovicheva, O., Demirdjian, B., Tishkova, V., Faccineto, A., Focsa, C., 2009. Characterisation of particulate matter and gaseous emissions from a large ship diesel engine. *Atmos. Environ.* 43 (16), 2632–2641. <http://www.sciencedirect.com/science/article/pii/S1352231009001253>.
- Najjar, R.G., Pyke, C.R., Adams, M.B., Breitburg, D., Hershner, C., Kemp, M., Howarth, R., Mulholland, M.R., Paolisso, M., Secor, D., Sellner, K., Wardrop, D., Wood, R., 2010. Potential climate-change impacts on the Chesapeake bay. *Estuar., Coast. Shelf Sci.* 86 (1), 1–20. <http://www.sciencedirect.com/science/article/pii/S0272771409004582>.
- Newsom, R.K., Turner, D.D., Mielke, B., Clayton, M., Ferrare, R., Sivaraman, C., Jul 2009. Simultaneous analog and photon counting detection for Raman lidar. *Appl. Opt.* 48 (20), 3903–3914. <http://ao.osa.org/abstract.cfm?URI=ao-48-20-3903>.
- Platt, U., Stutz, J., 2008. *Differential Optical Absorption Spectroscopy: Principles and Applications. Physics of Earth and Space Environments.* Springer, Berlin.
- Ring, A.M., Canty, T.P., Anderson, D.C., Vinciguerra, T.P., He, H., Goldberg, D.L., Ehrman, S.H., Dickerson, R.R., Salawitch, R.J., 2018. Evaluating commercial marine emissions and their role in air quality policy using observations and the cmaq model. *Atmos. Environ.* 173, 96–107. <http://www.sciencedirect.com/science/article/pii/S1352231017307033>.
- Sadanaga, Y., Fukumori, Y., Kobashi, T., Nagata, M., Takenaka, N., Bandow, H., NOV 15 2010. Development of a selective light-emitting diode photolytic NO₂ converter for continuously measuring NO₂ in the atmosphere. *Anal. Chem.* 82 (22), 9234–9239.
- Senff, C.J., Hardesty, R.M., Alvarez, R.J., Mayor, S.D., 1998. Airborne lidar characterization of power plant plumes during the 1995 southern oxidants study. *J. Geophys. Res.: Atmos.* 103 (D23), 31173–31189.
- Sillman, S., 1999. The relation between ozone, NO_x and hydrocarbons in urban and polluted rural environments. *Atmos. Environ.* 33, 1821–1845.
- Sinha, P., Hobbs, P.V., Yokelson, R.J., Christian, T.J., Kirchstetter, T.W., Brintjies, R., 2003. Emissions of trace gases and particles from two ships in the southern Atlantic ocean. *Atmos. Environ.* 37 (15), 2139–2148. <http://www.sciencedirect.com/science/article/pii/S1352231003000803>.
- Smit, H., Panel, A., 2011. *Global Atmospheric Watch Report No. 201.* Tech. Rep. World Meteorological Institution.
- Song, C.H., Chen, G., Hanna, S.R., Crawford, J., Davis, D.D., 2003. Dispersion and chemical evolution of ship plumes in the marine boundary layer: investigation of o₃/noy/hox chemistry. *J. Geophys. Res.: Atmos.* 108 (D4) n/a–n/a, 4143. <https://doi.org/10.1029/2002JD002216>.
- Stauffer, R.M., Thompson, A.M., Martins, D.K., Clark, R.D., Goldberg, D.L., Loughner, C.P., Delgado, R., Dickerson, R.R., Stehr, J.W., Tzortziou, M.A., Sep 2015. Bay breeze influence on surface ozone at edgewood, md during July 2011. *J. Atmos. Chem.* 72 (3), 335–353. <https://doi.org/10.1007/s10874-012-9241-6>.
- Steinbacher, M., Zellweger, C., Schwarzenbach, B., Bugmann, S., Buchmann, B., Ordonez, C., Prevot, A.S.H., Hueglin, C., JUN 12 2007. Nitrogen oxide measurements at rural sites in Switzerland: bias of conventional measurement techniques. *J. Geophys. Res.: Atmos.* 112 (D11).
- Sullivan, J.T., McGee, T.J., Sunnicht, G.K., Twigg, L.W., Hoff, R.M., Oct. 2014. A mobile differential absorption lidar to measure sub-hourly fluctuation of tropospheric ozone profiles in the Baltimore–Washington, D.C. region. *Atmos. Meas. Tech.* 7 (10), 3529–3548. <http://www.atmos-meas-tech.net/7/3529/2014/>.
- Sullivan, J.T., McGee, T.J., Thompson, A.M., Pierce, R.B., Sunnicht, G.K., Twigg, L.W., Eloranta, E., Hoff, R.M., Dec. 2015. Characterizing the lifetime and occurrence of stratospheric-tropospheric exchange events in the rocky mountain region using high-resolution ozone measurements. *J. Geophys. Res.* 120, 12.
- Sullivan, J.T., Berkoff, T., Gronoff, G., Knepp, T., Pippin, M., Allen, D., Twigg, L., Swap, R., Tzortziou, M., Thompson, A.M., Stauffer, R.M., Wolfe, G.M., Flynn, J., Pusede, S.E., Judd, L., Moore, W., Baker, B.D., Al-Saadi, J., McGee, T.J., 2019. The ozone water-land environmental transition study (owlets): an innovative strategy for understanding Chesapeake bay pollution events. *Bull. Am. Meteorol. Soc.* 0 (0) null. <https://doi.org/10.1175/BAMS-D-18-0025.1>.
- US Department of Commerce, N. O. A. A., 2018. NDBC station page. http://www.ndbc.noaa.gov/station_page.php?station=chbv2. http://www.ndbc.noaa.gov/station_page.php?station=CHBV2.
- Veefkind, J.P., Aben, I., McMullan, K., Förster, H., de Vries, J., Otter, G., Claas, J., Eskes, H.J., de Haan, J.F., Kleipool, Q., van Weele, M., Hasekamp, O., Hoogeveen, R., Landgraf, J., Snel, R., Tol, P., Ingmann, P., Voors, R., Kruijzinga, B., Vink, R., Visser, H., Levelt, P.F., May 2012. TROPOMI on the ESA Sentinel-5 Precursor: a GEMS mission for global observations of the atmospheric composition for climate, air quality and ozone layer applications. *Rem. Sens. Environ.* 120, 70–83.

- Villena, G., Bejan, I., Kurtenbach, R., Wiesen, P., Kleffmann, J., 2012. Interferences of commercial NO₂ instruments in the urban atmosphere and in a smog chamber. *Atmospheric Measurement Techniques* 5 (1), 149–159.
- Volten, H., Brinkma, E.J., Berkhout, A.J.C., Hains, J., Bergwerff, J.B., Van der Hoff, G.R., Apituley, A., Dirksen, R.J., Calabretta-Jongen, S., Swart, D.P.J., 2009. No₂ lidar profile measurements for satellite interpretation and validation. *J. Geophys. Res.: Atmos.* 114 (D24). <https://agupubs.onlinelibrary.wiley.com/doi/abs/10.1029/2009JD012441>.
- Wang, L., Newchurch, M.J., Alvarez II, R.J., Berkoff, T.A., Brown, S.S., Carrion, W., De Young, R.J., Johnson, B.J., Ganoe, R., Gronoff, G., Kirgis, G., Kuang, S., Langford, A.O., Leblanc, T., McDuffie, E.E., McGee, T.J., Pliutau, D., Senff, C.J., Sullivan, J.T., Sumnicht, G., Twigg, L.W., Weinheimer, A.J., Oct. 2017. Quantifying TOLNet ozone lidar accuracy during the 2014 DISCOVER-AQ and FRAPPÉ campaigns. *Atmos. Meas. Tech.* 10, 3865–3876.
- Williams, E.J., Lerner, B.M., Murphy, P.C., Herndon, S.C., Zahniser, M.S., 2009. Emissions of nox, so₂, co, and hcho from commercial marine shipping during Texas air quality study (texaqs) 2006. *J. Geophys. Res.: Atmos.* 114 (D21) n/a–n/a, d21306. <https://doi.org/10.1029/2009JD012094>.
- Winnes, H., Fridell, E., 2010. Emissions of nox and particles from manoeuvring ships. *Transportat. Res. Part D: Transp. Environ.* 15 (4), 204–211. <http://www.sciencedirect.com/science/article/pii/S136192091000012X>.
- Zhang, Y., Yi, F., Kong, W., Yi, Y., Nov 2014. Slope characterization in combining analog and photon count data from atmospheric lidar measurements. *Appl. Opt.* 53 (31), 7312–7320. <http://ao.osa.org/abstract.cfm?URI=ao-53-31-7312>.
- Zoogman, P., Liu, X., Suleiman, R., Pennington, W., Flittner, D., Al-Saadi, J., Hilton, B., Nicks, D., Newchurch, M., Carr, J., Janz, S., Andraschko, M., Arola, A., Baker, B., Canova, B., Miller, C.C., Cohen, R., Davis, J., Dussault, M., Edwards, D., Fishman, J., Ghulam, A., Abad, G.G., Grutter, M., Herman, J., Houck, J., Jacob, D., Joiner, J., Kerridge, B., Kim, J., Krotkov, N., Lamsal, L., Li, C., Lindfors, A., Martin, R., McElroy, C., McLinden, C., Natraj, V., Neil, D., Nowlan, C., OSullivan, E., Palmer, P., Pierce, R., Pippin, M., Saiz-Lopez, A., Spurr, R., Szykman, J., Torres, O., Veeffkind, J., Veihelmann, B., Wang, H., Wang, J., Chance, K., 2017. Tropospheric emissions: monitoring of pollution (TEMPO). *J. Quant. Spectrosc. Radiat. Transf.* 186, 17–39. satellite Remote Sensing and Spectroscopy: Joint ACE-Odin Meeting, October 2015. <http://www.sciencedirect.com/science/article/pii/S0022407316300863>.